Performance analysis of a dual component evaporator-absorber of an absorption heat transformer

J. Delgado-Gonzaga[a], A. Huicochea[a], J. Torres-Merino[b], I. Canela-Sánchez[a], D. Juárez-Romero[a],*

[a]*Centro de Investigación en Ingeniería y Ciencias Aplicadas, Universidad Autónoma del Estado de Morelos, Av. Universidad 1001, Col. Chamilpa, Cuernavaca, C. P. 62209, Morelos, México, email: javier.delgado@uaem.mx (J. Delgado-Gonzago), huico_chea@uaem.mx (A. Huicochea), justo_007@hotmail.com (I. Canela-Sánchez), Tel. (52-777) 3297984, email: djuarezr7@gmail.com (D. Juárez-Romero)*
[b]*Mezysep S.A. de C.V, 1a. Cerrada de Corcéles N° 9, Colina del Sur.,Ciudad de México C. P. 01430, email: jtorresmerino@gmail.com*

ABSTRACT

In this work, the behavior of a dual component evaporator-absorber (EV-AB) applied to an absorption heat transformer (AHT) operated with LiBr-H_2O is analyzed theoretically and experimentally. The purpose of this work is to obtain heat loads to improve the coefficient of performance (COP) of a thermodynamic cycle for water purification by distillation. The dual component EV-AB is composed of a chamber where processes of evaporation and absorption are carried out simultaneously. In both processes, heat transfer takes place by falling film. Internally there are two concentric vertical helical coils, which are fed by a refrigerant and an absorption mixture respectively by two independent drop distributors. The experimental results indicate that maximum amount of distilled water was 1.44 kg/h with a heat load in the absorber of 1.87 kW with a concentration of 55.24% by weight of LiBr-H_2O mixture to the inlet of the absorber. Regarding the COP of the AHT, a value close to 0.50 was registered. Experimental analysis indicates that the increase in the mass flow of refrigerant towards the evaporator, improves heat loads of the EV-AB. Through a mathematical model the effect of wetting efficiency of the evaporator was estimated, also is the analysis of wetting in the absorber shows the degradations of its heat transfer.

Keywords: Absorption heat transformer; Evaporator-absorber component; Falling film; Heat transfer; Heat transfer intensification

1. Introduction

Today, issues such as global warming, the growing demands for energy and environmental pollution, require the search for technologies to mitigate the extent of the problems. Absorption heat transformer (AHT) is one of the most promising technologies.

AHT is an energy-saving device that works in a thermodynamic cycle of absorption. It can reuse a low-grade thermal energy, such as solar energy and industrial waste heat, to produce useful high temperature heat, which can be reused in a secondary process [1]. The use of AHT can play a relevant role in increasing energy utilization efficiency. Fluids such as LiBr–H_2O and NH_3–H_2O are used as an absorbent mixture, which does not contribute to global warming or ozone depletion [2].

The AHT consists of a generator, a condenser, an evaporator, an absorber and an economizer (Fig. 1). The generator and condenser are located on the low-pressure side, while the absorber and evaporator are located on the high-pressure side. Waste heat is supplied to the generator and to the evaporator, while heat at an increased temperature is removed from the absorber [3].

The advantage of a heat transformer is that it may be used in any other system that requires a temperature greater

*Corresponding author.
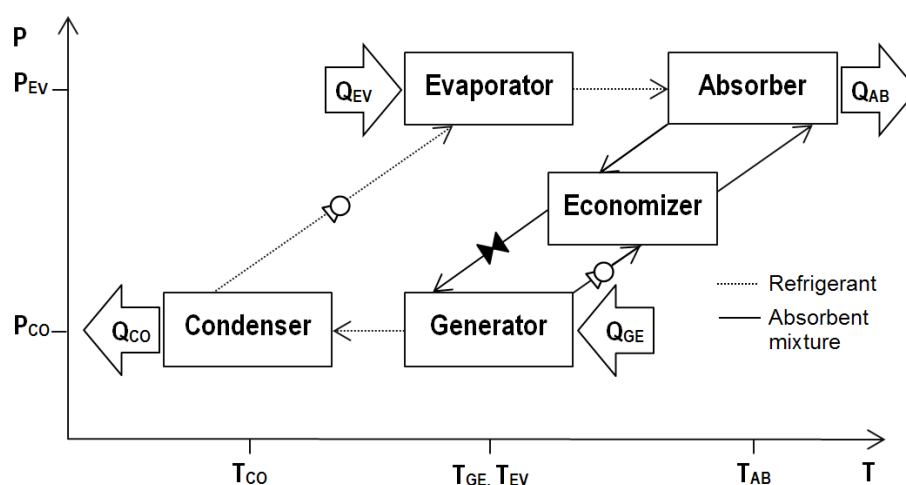
Fig. 1. Schematic diagram of a single stage AHT.

than the one provided by the source. With this advantage, published studies indicate that it is possible to integrate the water purification process to a heat transformer. This integration enables us to increase the temperature of the impure water system. Thus, pure water and useful heat are obtained [4].

It is important to work on designs that improve the performance of the AHT. Several geometries have been reported on heat exchangers applied to improve the performance of the AHT, such as vertical plates [5], falling film [6], disks shell and tube [7], and graphite [8], among others.

In the laboratory of applied thermal engineering at CIICAp-UAEM, work is aimed to design components that perform two unit operations in the same body to improve the performance of the AHT's. These types of devices (here called dual) have as design purposes: to reduce the dimensions of AHT's, to reduce investment costs, to prevent maintenance, as well as to reduce losses and time to stabilize the thermodynamic cycle.

Studies about dual components are limited, and those that exist are focused on absorption cooling systems [9–12].

This work consists of the theoretical, and experimental analysis of the dual component evaporator-absorber (EV-AB) applied to an AHT, with the purpose of obtaining: heat loads to improve the COP of the thermodynamic cycle and the water purification by distillation, through the application of useful heat from the absorber.

However, a problem to assess the performance of these dual components is the difficulty to measure some variables such as the wetting efficiency in the falling film, the mass flow of refrigerant evaporated per round, and the interfacial temperature accurately, which are involved in the process of mass and energy transfer [9]. A mathematical model was developed to estimate these variables and the internal behavior of EV-AB.

The experimental analysis of this AHT has been performed in two stages. The first stage was made by Morales et al. in 2015 [13,14], while the second one consists of 24 experimental tests analyzed in detail in this paper. Both experimental stages were studied with the same AHT, without changing the configuration of its elements.

Morales et al. in their study concluded that the EV is limited, due to low steam production, which results in low performance of the whole AHT. Based on these results, the coils of the EV and AB on its distributors were reoriented. Besides wires wrapped around every hole of the distributors were placed, to improve wetting and increase the values of heat loads in the dual component.

2. Description of the AHT-WP

The absorption heat transformer for water purification AHT-WP was designed for a capacity of 2 kW [15], and it is installed in the CIICAp (UAEM). Fig. 2 shows the general diagram of the AHT-WP with two dual components, GE-CO and EV-AB, where heat transfer takes place by falling film.

The GE-CO consists of two cylindrical stacked chambers connected by a lid that allows the flow of refrigerant desorbed in the GE towards the CO. Internally, the GE consists of two coils of the same number of rounds but with different winding diameter fed by a circular drop distributor through which the absorbent mixture flows. The CO is composed of two concentric coils of different diameter, which condenses the refrigerant.

The EV-AB is composed of a chamber where evaporation and absorption coils processes are performed. Internally there are two vertical concentric coils, which are fed refrigerant and absorbent mixture respectively, each by an independent distributor.

Each dual component has a peephole of borosilicate glass which allows monitoring the level of the absorbent mixture in each of the chambers at the time of the operation. The position of the experimental equipment is vertical to reduce the surface area as it is shown in Fig. 3.

An economizer is used to increase the heat level between the GE-CO and EV-AB. The economizer is a helical heat exchanger with a counter current configuration. This device recovers the heat of diluted absorbent mixture from the AB for the concentrated absorbent mixture which leaves the GE. Thus, the heat level is increased.
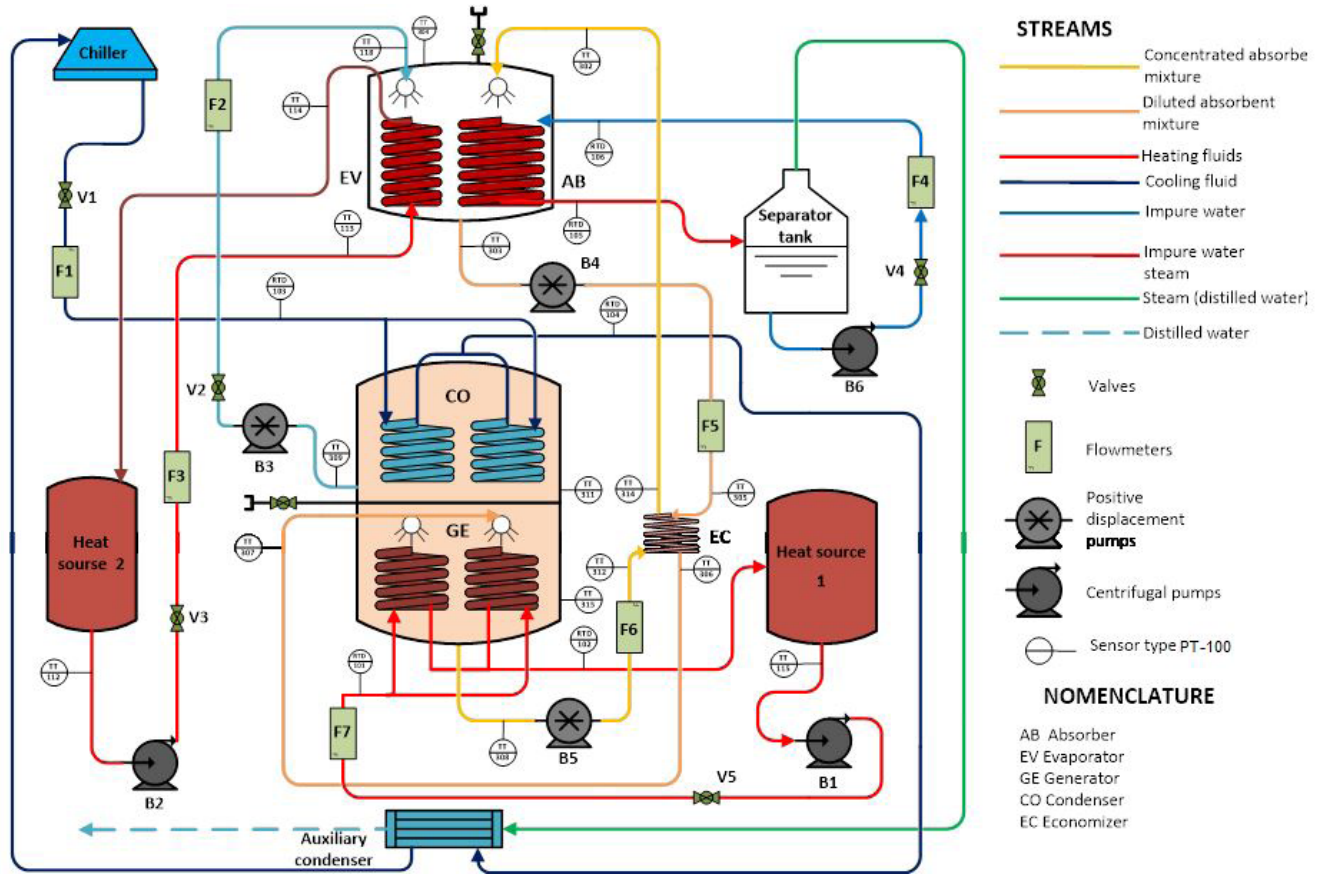
Fig. 2. General diagram of the AHT-WP.
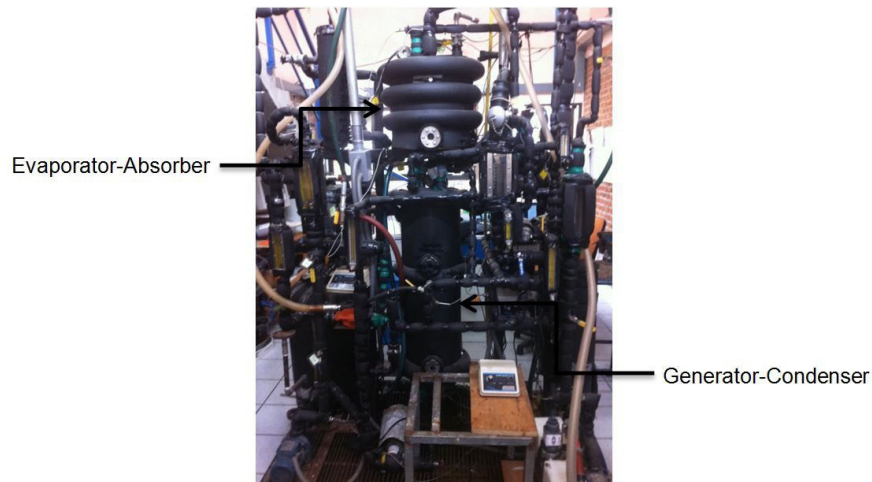
Fig. 3. Experimental AHT-WP.

The material used for the shell of the AHT components, coils of the heat exchangers, as well as tubes and fittings is stainless steel 316 L to reduce the effects of corrosion by lithium bromide. The AHT-WP is thermally insulated by elastomeric foam which has a thermal conductivity of 0.04 W/mK to minimize the loss of heat to the environment.

Two separate tanks that supply hot water by electric heaters simulate the heat source. The tank that supplies heat to GE is the heat source 1 and has three electric heaters with a total capacity of 9 kW, while the tank that supplies heat to the evaporator is the heat source 2 and has a total capacity of 5 kW. Each tank has a resistor connected to a voltage inverter to control the level of heat.

2.1. Operation of the AHT-WP

Initially, the tanks of heat sources (1 and 2) and the separator tank are filled with water. Afterwards, a water of heat source is heated by electrical resistance and pumped towards the GE and the EV. At the same time, the absorbent mixture between GE and AB is recycled, and the absorbent mixture level in both components is monitored through peepholes.

When absorbent mixture attains the saturation conditions in the GE, a phase change takes place: the refrigerant is desorbed from the GE. Then, the refrigerant travels toward the CO as superheated steam where it condenses by heat exchange with cooling water. This refrigerant is pumped to the EV as a saturated liquid and the phase changes to saturated steam which is absorbed by the concentrated absorbent mixture descending in the AB. Then, an exothermic reaction is carried out and impure water flowing inside the coil of AB takes the reaction heat. In the separator tank, steam leaves through the top and liquid water returns to the inlet of the AB. From the separator tank, the vapor circulates to an auxiliary condenser which yields heat to obtain distilled water as a product. Then, the diluted absorbent mixture leaves the AB, and it is directed to GE.

2.2. Design EV-AB

Internally, the dual component consists of a chamber with two concentric helical coils, where evaporation and absorption processes occur. The EV is placed in the internal part of AB, while the AB is placed in the external part, as can be seen in Fig. 4.

The shell of EV-AB is cylindrical, made of stainless steel plate 316 L schedule 8, internal diameter 34.64 cm and height 30 cm. The geometric characteristics of EV-AB appear in Table 1.

3. Thermodynamic analysis

The performance of the EV-AB in the AHT-WP was obtained applying the first law of thermodynamics to external circuits using the principles of mass and energy conservation. Heat balances, for the EV and AB at steady state conditions are as follows:

3.1. Heat load calculation

Evaporator. Heat supplied to the evaporator for the tube side is:

$$Q_{EV} = \dot{m}_{EV,Hw}\, Cp_{EV,Hw}\, (T_{EV,Hw,in} - T_{EV,Hw,out}) \tag{1}$$

Absorber. Heat obtained in the absorber. For the tube side is:

$$\dot{m}_{AB,Lw} = \dot{m}_{AB,Lw,out} + \dot{m}_{AB,DE} \tag{2}$$

$$\dot{m}_{AB,Lw}h_{AB,Lw,in} + Q_{AB} = \dot{m}_{AB,Lw,out}h^{LS}_{AB,Lw,out} + \dot{m}_{AB,DE}h^{VS}_{AB,DE} \tag{3}$$

Generator. Heat supplied to the generator for the tube side is:

$$Q_{GE} = \dot{m}_{GE,Hw}\, Cp_{GE,Hw}\, (T_{GE,Hw,in} - T_{GE,Hw,out}) \tag{4}$$

3.2. Coefficient of performance

When the pumping power is assumed negligible, the Coefficient of Performance (COP) is defined as the ratio between the heat delivered from the absorber and the heat load by the generator plus the evaporator:

Table 1
Geometric characteristics of the dual component EV-AB

	Evaporator	Absorber
Number of rounds	13	13
Coil winding diameter (m)	0.127	0.255
Tube length (m)	4.65	10.11
Tube internal diameter (m)	0.0111	0.0111
Tube external diameter (m)	0.0127	0.0127
Wall thickness (m)	0.0008	0.0008
Separation between rounds (m)	0.003	0.003
Coil height (m)	0.2	0.2
Heat transfer area (m²)	0.18	0.4

(a)   (b)
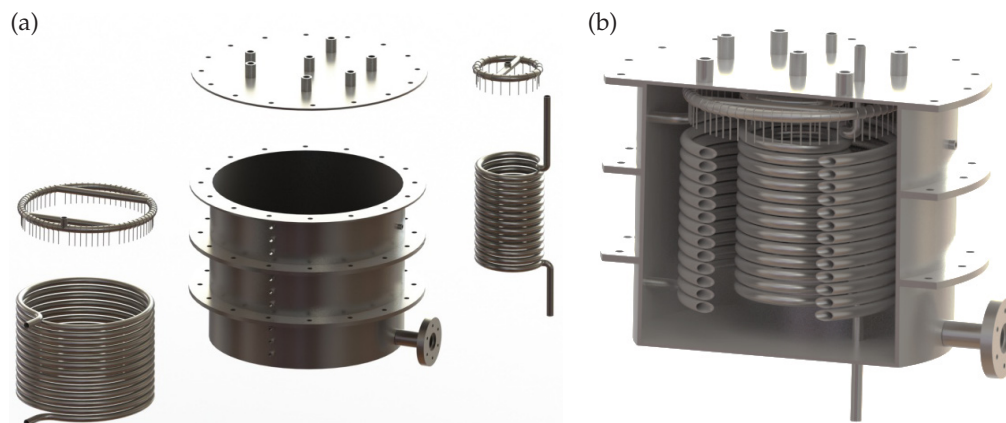
Fig. 4. Schematic view of the dual component EV-AB. (A) Component dismounted. (B) Component assembly.

$$COP_{AHT-WP} = \frac{Q_{AB}}{Q_{GE} + Q_{EV}} \qquad (5)$$

The absorbent mixture is Lithium Bromide, with water as a refrigerant. Correlations dependent on temperature and concentration evaluate the physical properties of the absorption mixture [16] Correlations dependent of pressure and enthalpy evaluated the physical properties of water [17].

4. Experimental methodology

The experimental data to determine the heat transfer of the dual component and COP, were obtained at steady state condition. This state is verified when in outlet temperatures of each component have variations of ± 1°C during 20 min.

Fig. 2 shows a schematic diagram of the AHT-WP, in which the location of the instruments used to quantify the variables involved in the analysis of the thermodynamic cycle, is observed.

To determine the temperature variable, twenty-eight PT-100 type sensors were installed along of the AHT-WP at the inputs and outputs of each of the main components. Two pressure transducers measure low and high pressure. Values of temperature and pressure were recorded at steady state, by means of a data acquisition system with two channel multiplexer modules.

Flow meters of different capacities were installed to measure and control the mass flow of the LiBr-H_2O mixture and the fluids of the auxiliary services. To circulate LiBr-H_2O mixture gear pumps of positive displacement were used; while centrifugal pumps were used for auxiliary service fluids. Impure water uses heat released from the absorber. Samples of the solution at the outlet of GE and AB are taken and analyzed by a refractometer to determine the concentration with a correlation reported by Holland et al. [18].

5. Results and discussion

Based on the experimental analysis conducted by Morales in 2015 [14], it was decided to focus these tests on the variation of the value of the mass flow of refrigerant that feeds the evaporator. After wire was wrapped around every hole of the distributors, and the coils were re-oriented with respect to its distributors, then we evaluated the heat loads of the dual component EV-AB;

Those that satisfied the requirements for steady state condition are presented.

5.1. Experimental analysis

Fig. 5 shows the experimental test during three operating states: the preheating, transient and steady state. Absorber plot is presented because this is the last component of the AHT-WP to stabilize, due to the interaction the AB has with the GE. Fig. 5 shows the experimental test which required a short period to reach the stability conditions.

The first state is the preheating state, in which the stream temperatures increase because in this period it is when the
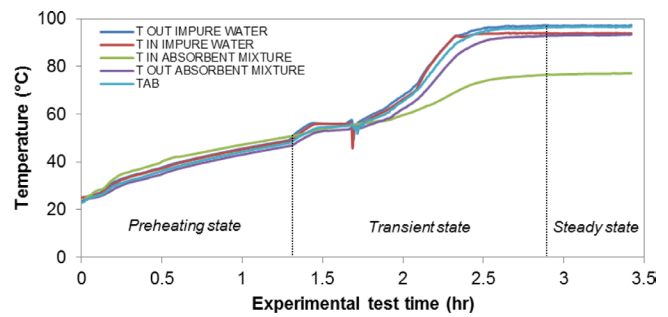
Fig. 5. Behavior of streams temperatures of the AB in an experimental test.

auxiliary services supply heat to the AHT-WP to start the thermodynamic cycle. The duration of the preheat state in this test lasted 1.3 h approximately.

The second state corresponds to the transient state in which the AB is pressurized, because of the evaporation process. Also, the temperature increases because of the released heat in the absorber, as observed in Fig. 5, through the immediate increment of the stream temperatures. The period of this state lasted 1.5 h approximately.

The last state corresponds to the steady state. At this state the AB and AHT-WP in general, have reached the thermodynamic equilibrium. At this state, distilled water is obtained as the product of the useful heat released from the exothermic reaction. At this state the values of the stream temperatures in AB do not vary ± 1°C. After 2.8 h AB reached stability for this experimental test.

Fig. 6 shows the behavior of Q_{AB} as a function of Q_{EV}; while $\dot{m}_{Ref}$ is represented by bubble size. When $\dot{m}_{Ref}$ increases in experimental tests, an upward trend in Q_{EV} is observed due to an increase in differential enthalpy [Eq. (1)] for the evaporation process. While in the Q_{AB}, the tendency of the heat load is due to the increased amount of refrigerant (saturated steam) which benefits the amount of heat released from the exothermic reaction.

The results presented by Morales et al. [14] in a previous experimental stage with this AHT-WP indicate that the maximum values obtained were 0.91 and 0.19 kW for the EV and AB. The results of the present stage as shown in Fig. 6 indicate the maximum values obtained were 1.59 and 1.87 kW in the EV and the AB. These results show
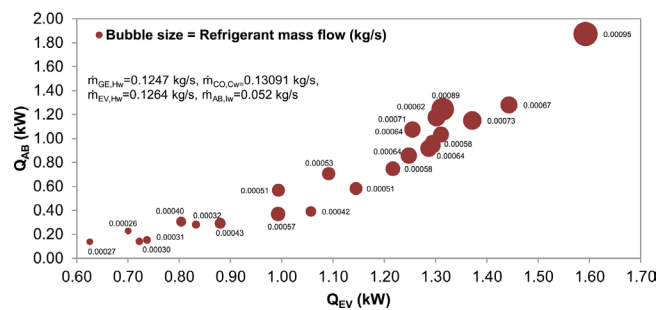
Fig. 6. Behavior of the evaporator heat load Q_{EV} regarding the absorber net load Q_{AB} along the experimental tests of this work. While the circles represent the refrigerant mass flow $\dot{m}_{Ref}$.

that the re-orientation of the coils on its distributors and wire wrapped around every hole of the distributors, have a substantial improvement in the heat loads of the dual component.

Operating conditions for the heat loads of Fig. 6 are varied, and a summary thereof is presented in Table 2.

Fig. 7 shows the behavior of $\dot{m}_{DE}$ as a function of $\dot{m}_{Ref}$. The distillation process is carried out at ambient conditions of UAEM. They correspond to a saturation temperature of 94.1°C and pressure 81.86 kPa.

When a greater amount of Q_{AB} is obtained, the sensible heat decreases while the latent heat increases, favoring the amount of distilled water.

The highest rate of $\dot{m}_{DE}$ was 1.44 kg/h with $\dot{m}_{Ref}$ of 0.00095 kg/s. It is noteworthy that distillates obtained in this work are first for this AHT-WP.

Fig. 8 shows the behavior of the COP as a function of the heat load of the AB. The uncertainty of COP values was considered equal to ±15.4%. This value of uncertainty is taken from the analysis of an AHT with similar instrumentation [19].

It has been determined through experimental analysis that $\dot{m}_{Ref}$ is a limiting variable in this thermodynamic cycle, since as the value of this variable increases, also Q_{EV} and Q_{AB} increases. However, despite the increase of both, Fig. 8 indicates that heat load released in the absorber increases in a higher proportion on heat supplied to the AHT-WP [Eq. (4)], which it is reflected in the upward trend of the COP.

Morales et al. presented a maximum value of COP of 0.35 [14]. While the results of this stage as shown in Fig. 8 indicate that the maximum value of COP was close to 0.50 with an absorber heat load of 1.6 kW.
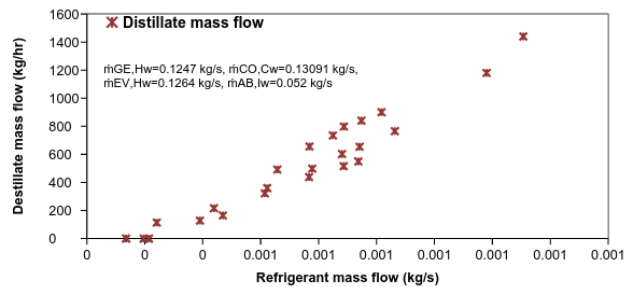
Fig. 7. Behavior of the distillate mass flow $\dot{m}_{DE}$ as a function of the refrigerant mass flow $\dot{m}_{Ref}$, along the experimental tests of this work.
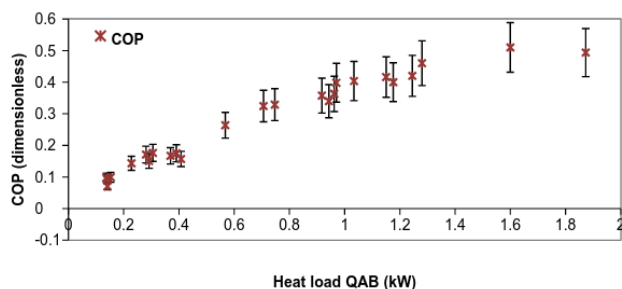
Fig. 8. Behavior of the COP as a function of the absorber heat load Q_{AB}, along the experimental tests of this work.

Table 2 shows the range of operating conditions of the tests conducted in this work, as well as the operating conditions of the test in which the maximum heat load for the evaporator and absorber were obtained. $T_{EV,Ref,out}$ was calculated as a function of the absolute pressure of the EV-AB.

5.2. Results derived from the mathematical model

Due to the complexity of the component geometry, a mathematical model was developed to estimate the vari-

Table 2
Summary of experimental operating conditions in the EV-AB

Variable	Operation range	Operating conditions for the maximum Q_{AB}
Temperature (°C)		
$T_{GE,Hw,in}$	88.28–68.36	88.28
$T_{GE,Hw,out}$	84.09–66.31	84.09
$T_{EV,Hw,in}$	80.50–73.20	80.50
$T_{EV,Hw,out}$	77.50–71.68	77.50
$T_{EV,Ref,in}$	37.64–27.09	37.64
$T_{EV,Ref,out}$	71.32–51.03	71.32
T_{EV}	71.32–51.03	71.32
$T_{AB,Iw,in}$	94.70–91.16	94.31
$T_{AB,Iw,out}$	98.74–91.81	98.74
$T_{AB,Sln,in}$	76.83–66.81	75.35
$T_{AB,Sln,out}$	94.11–86.65	94.11
$T_{AB,Ref,in}$	71.32–51.03	71.32
T_{AB}	98.26–90.70	97.68
Mass flow (kg/s)		
$\dot{m}_{EV,Hw}$	0.1264	0.1264
$\dot{m}_{EV,Ref,in}$	0.00095–0.00027	0.00095
$\dot{m}_{EV,Ref,out}$	0.00095–0.00027	0.00095
$\dot{m}_{AB,lw}$	0.052	0.052
$\dot{m}_{AB,Sln,in}$	0.02385–0.01407	0.01476
$\dot{m}_{AB,Sln,out}$	0.02451–0.01480	0.01557
$\dot{m}_{AB,Ref,in}$	0.00095–0.00027	0.00095
$\dot{m}_{DE}$	0.00040–0.00000	0.00040
Concentrations (%)		
$x_{AB,in}$	58.34–54.15	55.24
$x_{AB,out}$	56.72–50.18	51.29
Pressure (kPa)		
P_{EV}, P_{AB}	33.04–13.00	33.04
Heat load (kW)		
Q_{EV}	1.59–0.63	1.59
Q_{AB}	1.87–0.14	1.87
COP (dimensionless)		
COP	0.50–0.07	0.49

ables that are not possible to measure experimentally. The assumptions and specifications of the model are presented in Appendix A.

As the flow is evaporated, the wetting efficiency is expected to decrease linearly on the film Reynolds $Re_\Gamma = \dfrac{4\Gamma}{\mu}$ for one-set dry-out. This Reynolds for onset dry-out was fitted so that the heat of the evaporator matched the experimental value of the heat supplied.

Fig. 9 shows that even the first rounds of the coil were not fully wetted. As the refrigerant is evaporated, the wetting efficiency decreases asymptotically, but part of the refrigerant is not evaporated.

Works on humidification efficiency in absorber are reported by Jeong and Garimella [20]. Wetting efficiency was varied in the mathematical model in a range of 30–45%. The range of wetting efficiency selected here was taken from the reported values of the falling film helical generator for this AHT [21].

Fig. 10 shows the temperature of the falling film (LiBr-H_2O), in each round of the absorption coil, at different values of wetting efficiency. This figure shows that, if wetting efficiency is reduced from 0.45 to 0.30, the outlet absorbent mixture temperature increases from 95.98 to 96.12°C, since the released heat is not transferred to the impure water.

6. Conclusions

This work presented the theoretical-experimental analysis of the dual component EV-AB, applied to a thermal
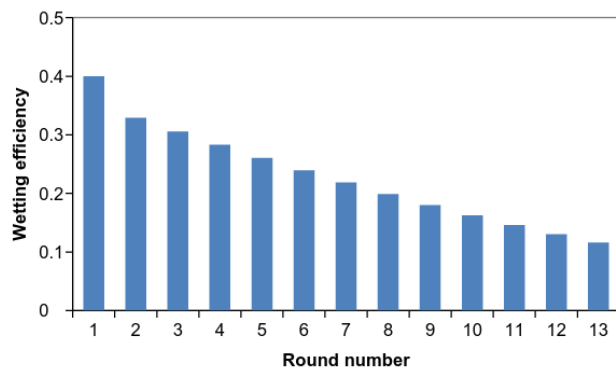
Fig. 9. Estimated wetting efficiency per round of the evaporator.
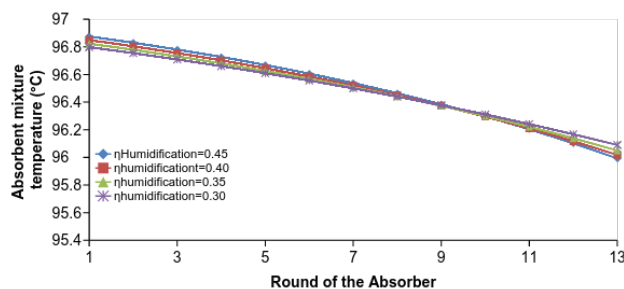
Fig. 10. Absorbent mixture temperature by tube of the absorber, varying the average wetting efficiency in the absorber *n*.

transformer for water purification AHT-WP. The re-orientation of the coils on its distributors and wire wrapped around every hole of the distributors have a considerable benefit in the heat loads of the dual component and COP of the thermodynamic cycle.

With a concentration of 55.24 by weight of LiBr-H_2O mixture to the inlet of the absorber, a maximum was 9.5 ×10⁻⁴ kg/s with heat loads of Q_{EV} = 1.59 kW and Q_{AB} = 1.87 kW. These heat loads show an appropriate balance for a duplex component. At this condition, the COP was close to 0.5. Also, during the production state a maximum flow of 1.44 kg/h of distilled water was obtained.

The mathematical model has been useful to show that for a compact design in the evaporator, it is more convenient to have a larger value of area per round since there is a steady decrement of the wetted surface as the refrigerant descends through the coil structure. In the absorber, the computer model shows that as the overall wetting efficiency is reduced, the temperature of the absorber remains almost constant.

Symbols

$\dot{m}$	—	Mass flow, kg/s
A	—	Heat transfer area, m²
COP	—	Coefficient of performance, dimensionless
Cp	—	Heat capacity, kJ/kg°C
Dm	—	Tube diameter, m
F	—	Flowmeter
h	—	Enthalpy, kJ/kg
h	—	Hours
L	—	Length, m
P	—	Pressure, kPa
Q	—	Heat load, kJ/s
s	—	Separation between the tubes, m
T	—	Temperature, ° C
U	—	Overall heat transfer coefficient, kW/(m²°C)
V	—	Valves
X	—	Composition, % wt.

Greek

α	—	Heat transfer coefficient, kW/m²
δ	—	Film thickness, m
Γ	—	Flow per unit length, kg/s m
λ	—	Latent heat, kJ/kg
μ	—	Viscosity, kg/ms
η	—	Efficiency
ρ	—	Density, kg/m³
θ	—	Angle, rad

Subscripts

AB	—	Absorber
abso	—	Absorption
Avg	—	Average
conv	—	Convective
Cw	—	Cooling water
DE	—	Distilled water
EV	—	Evaporator
ext	—	External

f   — Film
Hlc   — Coil
Hw   — Heating water
I   — Inner
in   — Input
Iw   — Impure water
O   — Outer
out   — Output
p   — Round
Ref   — Refrigerant
s   — Saturation
Sln   — Absorbent mixture
Tot   — Total
tran   — Transfer
wet   — Wetting
wll   — Wall

Superscripts

Ls   — Saturated liquid
Vs   — Saturated vapor

Acronyms

AB   — Absorber
AHT-WP   — Absorption heat transformer for water purification
Ar   — Archimedes number based on tube diameter
CO   — Condenser
EC   — Economizer
EV   — Evaporator
Ga   — Galileo number
GE   — Generator
Nu   — Nusselt number
Pe   — Peclet number = Re Pr
Pr   — Prandtl number
Re   — Reynolds number

References

[1] R. Ren, Z. Zhao, X. Zhang, Vapor pressures, excess enthalpies, and specific heat capacities of the binary working pairs containing the ionic liquid 1-ethyl-3-methylimidazolium dimethylphosphate, J. Chem. Thermodyn., 43 (2011) 576–583.
[2] E.K. Herold, R. Radermacher, S.A. Klein, Absorption Chillers and Heat Pumps, CRC Press, Inc., Boca Raton, Florida, (1996).
[3] K. Parham, M. Khamooshi, D. Boris, K. Tematio, M. Yari, U. Atikol, Absorption heat transformers – A comprehensive review, Renew. Sustain. Energy Rev., 34 (2014) 430–452.
[4] J.A. Hernández, D. Juárez-Romero, L.I. Morales, J. Siqueiros, COP prediction for the integration of a water purification process in a heat transformer: with and without energy recycling, Desalination, 219 (2008) 66–80.
[5] M. de Vega, J.A. Almendros-Ibañez, G. Ruiz, Performance of a LiBr–water absorption chiller operating with plate heat exchangers, Energy Convers. Manage., 47 (2006) 3393–3407.
[6] M. Medrano, M. Bourouis, A. Coronas, Absorption of water vapour in the falling film of water–lithium bromide inside a vertical tube at air-cooling thermal conditions, Int. J. Thermal Sci., 41 (2002) 891–898.
[7] J.I. Yoon, E. Kim, K.H. Choi, W.S. Seol, Heat transfer enhancement with a surfactant on horizontal bundle tubes of an absorber, Int. J. Heat Mass Transf., 45 (2002) 735–741.
[8] J. Olarte-Cortés, J. Torres-Merino, J. Siqueiros, Experimental study of a graphite disks absorber couple to a heat transformer, Experim. Thermal Fluid Sci., 46 (2013) 29–36.
[9] Y. Chen, C.-Y. Sun, Experimental study on the heat and mass transfer of a combined absorber-evaporator exchanger, Int. J. Heat Mass Transf., 40 (1997) 961–971.
[10] I.P. Tsern, H.I. Lin, S.F. Chou, Heat and mass transfer in the vertical twin parallel-tube absorber-evaporator unit, J. Chin. Inst. Eng., 24 (2001) 581–593.
[11] G.A. Florides, S.A. Kalogirou, S.A. Tassou, L.C. Wrobel, Design and construction of a LiBr–water absorption machine, Energy Conv. Manage., 44 (2003) 2483–2508.
[12] J. Pospisil, M. Balas, M. Baxa, Z. Fortelny, Working characteristics of small-scale absorption unit with two-cylinder design, WSEAS Trans. Heat Mass Transfer, 3 (2009) 77–86.
[13] L.I. Morales, Design, construction and experimental evaluation of an Absorption Heat Transformer with duplex components of 2 kW (Doctoral Thesis), CIICAp, Cuernavaca, Morelos, 2015 (in Spanish).
[14] L.I. Morales, R.A. Conde-Gutiérrez, J.A. Hernández, A. Huicochea, D. Juárez-Romero, J. Siqueiros, Optimization of an absorption heat transformer with two-duplex components using inverse neural network and solved by genetic algorithm, Appl. Thermal Eng., 85 (2015) 322–333.
[15] N. Demesa, Design and Construction of a Duplex Heat Exchanger for Absorption Heat Transformer (Master Thesis), CIICAp, Cuernavaca, Morelos, 2012 (in Spanish).
[16] J. Torres Merino, Contacteurs gaz-liquide pour pompes à chaleur à absorption multi-étages (Doctoral Thesis), L'institut national polytechnique de Lorraine, France, 1997.
[17] M. Holmgren, Xsteam: Water and steam properties according to IAPWS IF-97, www.x-eng.com, 2007.
[18] F.A. Holland, J. Siqueiros, S. Santoyo, C.L. Heard, E.R. Santoyo (Eds.), Water Purification Using Heat Pumps, E & FN Spon/Routledge, London and New York, 1999.
[19] M. Meza, A. Márquez-Nolasco, A. Huicochea, D. Juárez-Romero, J. Siqueiros, Experimental study of an absorption heat transformer with heat recycling to the generator. Exper. Thermal Fluid Sci., 53 (2014) 171–178.
[20] S. Jeong, S. Garimella, Falling-film and droplet mode heat and mass transfer in a horizontal tube LiBr/water absorber, Int. J. Heat Mass Transf., 45 (2002) 1445–1458.
[21] Y. Lazcano-Véliz, J.A Hernández, D Juárez-Romero, A. Huicochea-Roriguez, A. Alvarez-Gallegos, J. Siqueiros (2016) Improved of effective wetting area and film thickness on a concentric helical bank of a generator for an absorption heat transformer, Appl. Thermal Eng., 106 1319–1328
[22] J.J. Lorenz, D. Yung, A note on combined boiling and evaporation of liquid films on horizontal tubes. Trans. ASME, 101 (1979) 178–180.
[23] X. Hu, A.M. Jacobi, The intertube falling film: Part 1—Flow characteristics, mode transitions, and hysteresis, J. Heat Transf., 118(3) (1996) 616–625.
[24] X. Hu, A.M. Jacobi, The intertube falling film: Part 2—Mode effects on sensible heat transfer to a falling liquid film, J. Heat Transf., 118(3) (1996) 626–633.
[25] W. Li, X. Wu, Z. Luo, R.L. Webb, Falling water film evaporation on newly-designed enhanced tube bundles, Intl. J. Heat Mass Transf., 54(11) (2011) 2990–2997.
[26] G. Ribatski, J.R. Thome, Experimental study on the onset of local dryout in an evaporation falling film on horizontal plain tubes, Exper. Thermal Fluid Sci., 31 (2007) 483–493.
[27] M. Habert, J.R. Thome, Falling-film evaporation on tube bundle with plain and enhanced tubes—Part II: New prediction methods, Exper. Heat Transf., 23(4) (2010) 281–297.
[28] M.J. Kirby, H. Perez-Blanco, A design model for horizontal tube water/litihium bromide absorbers, Heat Pump Refrige. Sys. Design AES, 32 (1994) 1–10.
[29] J.S. Seewald, H. Perez-Blanco, A Simple model for calculating the performance of a lithium-bromide/water coil absorber, ASHRAE Trans., 100 (1994) 318–328.

Appendix A

A.1.1. Assumptions of model of the evaporator

- The refrigerant produces no splashes when it touches the tubes of the evaporator.
- The wetting efficiency depends quasi-linearly on film Reynolds, since film Re is small.
- The temperature of the tube wall is uniform in every round of the coil.
- The evaporation takes place at the inter-phase.
- There is no nucleate boiling in the film.
- The evaporated steam is sufficient to fill the absorption chamber. Thus, the effect of un-wetted areas of the evaporator tubes is diminished.
- The energy losses to the environment are negligible.

A.1.2. Energy balances

The balances used in the model for the evaporator are as follows:

$$\dot{m}_{EV,in,p} = \dot{m}_{EV,out,p} + \dot{m}_{EV,Ref,p} \tag{6}$$

Energy balance:

$$\dot{m}_{EV,in,p}h_{EV,in,p} + \alpha_{EV,f,p}\eta_{EV,f,p}(T_{EV,w,p} - T_{EV,Ref,S})$$
$$= \dot{m}_{EV,out,p}h^{LS}_{EV,out,p} + \dot{m}_{EV,Ref,p}h^{VS}_{EV,Ref,p} \tag{7}$$

A.1.3. Heat transfer coefficients

The accurate estimation of the falling film heat transfer in the evaporator is important, not only because this coefficient limits the heat transfer in the evaporator (since in the tube-side the flow is turbulent, and its performance is enhanced by the coiled shape); but also, because the released absorption heat is directly related to the steam production.

Lorenz & Yung [22] observed that the performance of the heat transfer depends on $Re_\Gamma = \frac{4\Gamma}{\mu}$:

At $Re_\Gamma < 30$ dry patches occur. α_f increases as Re_Γ, wetting, increases.

At $30 < Re_\Gamma < 100$ film thickness dominates heat transfer. α_f decreases slightly as Re_Γ increases

At $100 < Re_\Gamma$ turbulence dominates heat transfer. α_f increases as Re_Γ increases.

The work of Hu & Jacobi [23,24] describes the effect of film evaporation in a bank of tubes at different flow patterns at different values of the Galileo and Reynolds numbers. The flow pattern identified, for the operating conditions of the AHT, was droplet mode:

$$Droplet\ mode\ Nu = 0.113\ Re^{0.85}Pr^{0.85}Ar^{-0.27}\left(\frac{s}{Do}\right) \tag{8}$$

Li et al. [25] observed that this correlation does not predict the change of trend of their experimental results during the transition of Reynolds number from partially dry out to fully wet.

In the evaporator of the present work, $Re_\Gamma \leq 15$, and decreases as the refrigerant evaporates, thus, wetted surface decreases.

Ribatsky & Thome [26] suggest, that for film evaporation under dry-out conditions

$$\alpha_{f,p} = \alpha_{wet,p}\eta_{wet,p} + \alpha_{conv,p}(1 - \eta_{wet,p}) \tag{9}$$

The wetted film side film transfer coefficient is approximated by the Nusselt theory:

$$\alpha_{wet,f,p} = \frac{k}{\delta p} \tag{10}$$

Here $\delta_p = \left(\frac{3\mu\Gamma_p}{\rho^2 gsin(\theta_{avg})}\right)$, also: $\Gamma_p = \frac{\dot{m}}{2L_p}$

The α_{conv} represents the convection heat transfer. This value is small compared with $\alpha_{wet.}$

In this work, we use the approximation, see Habert &Thome [27]:

$$\eta_{EV,Wet,p} = \frac{A_{wet,p}}{A_{Tot}} \approx \frac{Re_{\Gamma,p}}{Re_{\Gamma,0}} \tag{11}$$

$Re_{\Gamma,0}$, the one set dry-out Reynolds, this is an important parameter for the wetting performance. In work, this value is selected as a fitting parameter to match the heat transfer supplied.

The tube side heat transfer is evaluated by the Dittus-Boetler correlation;

$$Nu_i = \frac{D_i\alpha_i}{\kappa} = 0.026\ Re^{0.8}\ Pr^{0.3} \tag{12}$$

For a helical coil Nusselt is enhanced as

$$Nu_{hlc} = Nu\left[1 + 3.5\left(\frac{D_o}{D_{hlc}}\right)\right]$$

Then

$$\frac{1}{UA\eta_{wet}} = \frac{1}{\alpha_f A\eta_{wet}} = \frac{1}{\alpha_i A_i} \tag{13}$$

$$Q_{EV,tran,p} = U\eta_{EV,tran,p}A_{EV,p}(T_{EV,Hw,p} - T_{EV,Ref,p}) \tag{14}$$

A.2. Assumptions of the model of the absorber

- The absorption starts as soon as the absorption mixture stream gets in contact with the refrigerant steam.
- The absorption mixture arrives at the distributor without splashes.
- The main flow of through the coil is cross current.
- A wetting efficiency is due to splashes, and non-uniform film distribution
- The impure water arrives at the saturation conditions.

• The evaporation inside the absorber tubes has little effect in heat transfer (since the evaporated fraction is small there).

A.3. Energy balances

The balances used in the model for the absorber are as follows, for every round, *p* (Eq. (6))
Mass balance:

$$\dot{m}_{AB,sln,in,p} + \dot{m}_{AB,Ref,in,p} = \dot{m}_{AB,sln,out,p} \tag{15}$$

Energy balance:

$$\dot{m}_{AB,sln,in,p} h_{AB,sln,in,p} + \dot{m}_{AB,Ref,in,p} h_{AB,Ref,in,p}$$
$$= \dot{m}_{AB,sln,out,p} h_{AB,sln,out,p} + Q_{AB,tran} \tag{16}$$

And the heat load is defined by:

$$Q_{AB,tran,p} = U_{AB} A_{AB,p} \eta_{AB,Wet} (T_{Ab,sln,p} - T_{Ab,lw,p}) \tag{17}$$

A.2.3. Heat transfer coefficients

In the film side, the work of Kirby & Perez-Blanco [28], refers to film cross-flow open contact of lithium bromide with hot water as a heating fluid. The dependence on Re, Pr, and film thickness corresponds to laminar flow for cross current contact.

$$Nu_f = 1.03 \left(\frac{Pe\delta}{2\pi D_o} \right)^{0.4} \tag{18}$$

Also, Seewald and Perez-Blanco [29] developed a model for the heat transfer for a horizontal coil. They estimated the effective wetting area from the aspect slope (D_o/D_{Hlc} = 0.111) and the contact angle between the absorption mixture-wall. In the present work the aspect slope is smaller (D_o/D_{Hlc} = 0.05). Thus the correlation by Kirby and Perez-Blanco was selected.

Inside the tubes, the heat transfer is turbulent; the Dittus-Boelter correlation was used. In the tubes of the absorber, only sensible heat was considered.

The Nusselt number was also corrected for the fluid inside the tubes.